Dalton Transactions

PAPER

View Article Online
View Journal | View Issue

Cite this: *Dalton Trans.*, 2019, **48**, 15127

A new set of metal–organic frameworks synthesised from diisophthalate-based, 2′-phosphorus-substituted *m*-terphenyl linker molecules†

Timo Stein, Frank Hoffmann and Michael Fröba *

Four metal–organic frameworks employing the *m*-terphenyl diisophthalate linker molecule with 2′ substitution by P(v)-based functional groups of the central aryl have been synthesised. The dense packing of $POMe_2$/$PSMe_2$ functional groups within **UHM-60**/**UHM-61** (UHM: University of Hamburg Materials) with an underlying net of **ucp** topology was overcome by increasing the sterical demand of phosphorus substituents. Replacement of the $PEMe_2$ (E = O, S) functional groups by $POEt_2$ or $POPh_2$ gave **UHM-62** and **UHM-63**, respectively, where valid deconstructions of the underlying topology to types 3,3,4,4T199, **tim**, and **tst** were found. The potential influence of the now-accessible phosphoryl functional group towards CO_2 and CH_4 adsorption as well as the selectivity towards CO_2/CH_4 separation was studied. Based on a comprehensive survey of literature-known Cu(II)-based MOFs with *m*-terphenyl-based linker molecules, we propose the deconstruction of inter-isophthalate plane angles to angular components of twist and fold allowing for the sophisticated classification of topologies that can be realised in Cu(II)-based MOFs using the *m*-terphenyl tetracarboxylate linker molecule.

Received 25th July 2019,
Accepted 23rd September 2019

DOI: 10.1039/c9dt03044a

rsc.li/dalton

Introduction

We are interested in the synthesis of metal–organic frameworks (MOFs) with organic linker molecules bearing phosphorus-based functional groups with special attention to (a) the relationship between functional groups and the topology of the underlying net of MOFs obtained and (b) chemical utilisation of the phosphorus chemical group by means of post-synthetic metalation and subsequent applications in catalysis. We decided on using the *m*-terphenyl structural motif as a linker backbone for the phosphorus-based functional groups attached to the C2′ position of the central aryl, see Fig. 1. The connectivity to the respective inorganic secondary building unit was intended to be realised *via* carboxylates provided by isophthalate functional groups of the parent bent diisophthalate.

With special emphasis on P(III)-based phosphanes, phosphorus-based ligands are among the most commonly employed ligands in the fields of organometallic and coordination chemistry. Their coordinating properties towards Lewis acids can be fine-tuned over a broad range by means of well-established methods of synthetical chemistry, influencing both steric and electronic properties.[1] Moreover, the transition to phosphane oxides and phosphane sulfides alters the Lewis basicity dramatically, rendering those reagents useful as solvating metal extractants in the area of hydrometallurgy.[2] Bulky *m*-terphenyls form a rigid and concave backbone that has been employed to stabilise both 2′-attached phosphane ligands as well as derived transition metal complexes towards oxidation and dissociation reactions, respectively.[3]

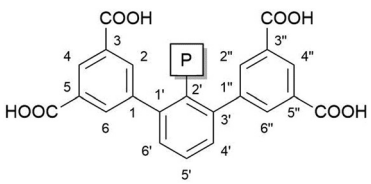

Fig. 1 The diisophthalate-based *m*-terphenyl linker molecule backbone with a C2′-attached phosphorus functional group. The numbering system of the ligand backbone is given.

Institut für Anorganische und Angewandte Chemie, Universität Hamburg, Martin-Luther-King-Platz 6, 20146 Hamburg, Germany.
E-mail: michael.froeba@chemie.uni-hamburg.de

†Electronic supplementary information (ESI) available: Synthetical details, analytical methods, *in silico* methods, preparation and characterisation of organic molecules and MOFs, literature survey concerning *m*-terphenyl diisophthalate coordination polymers and single crystal data. CCDC 1942981–1942987, 1942989 and 1942990. For ESI and crystallographic data in CIF or other electronic format see DOI: 10.1039/c9dt03044a

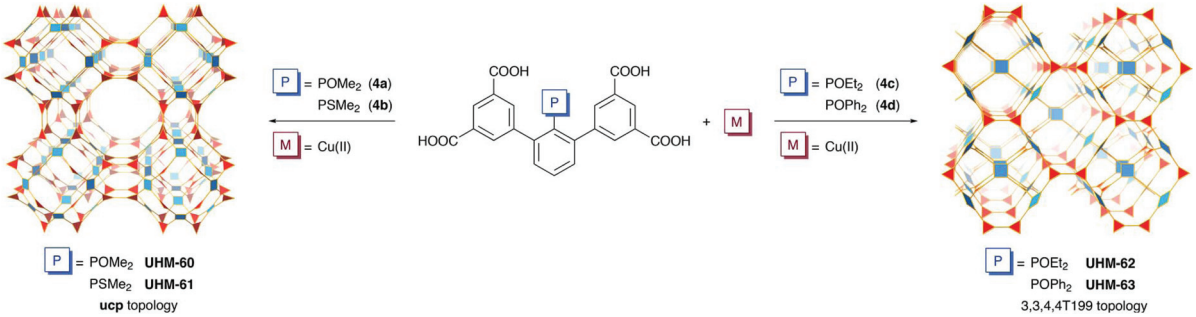

Fig. 2 The 2′-phosphorus substitutional motifs of the parent *m*-terphenyl tetracarboxylic acid linker molecules along with the metal ions used for the synthesis of the UHM MOFs presented within this work. The MOFs are represented by the respective augmented versions of their underlying nets. Only one possibility of the underlying net of **UHM-62** and **UHM-63** is shown.

The *m*-terphenyltetracarboxylate motif has been employed in the synthesis of a large number of MOFs, the majority of which were Cu(II)-based systems (see Table S4†) like the well-known **PCN-305**[4]/**NJU-Bai10**[5] or one of the numerous examples belonging to the **ZJNU** series.[6] However, concerning the 2′ position of the linker molecule, only examples exhibiting aza-substitution[7–9] or substitution by structurally simple substituents like amino[10–13] or methyl groups[6,14] have come to our attention.

Some P(v)-based frameworks reported to date show exceptional CO_2 uptakes,[15] while the variety of linker molecules employed was, apart from only few notable exceptions,[16,17] limited to the tri(4-carboxyphenyl)phosphane oxide linker molecule or its elongated analogues.[18–20] The P═O functional group was shown to coordinate to the secondary building unit or metal ion *via* oxygen especially in cases where harder metal ions were employed.[21–23] In case of the medium-hard Cu(II) ion, only two MOFs with the P═O oxygen atom being coordinated[24] and uncoordinated,[25] respectively, were reported.

We have synthesised a series of P(v)-based phosphane oxide and phosphane sulfide linker molecules. We felt that substitution by sterically demanding P-based functional groups at the 2′ position might enable for the synthesis of structurally and topologically novel Cu(II) MOFs and intended to investigate whether the combination of open metal sites[26] and polar phosphane oxide functional groups might be beneficial in terms of CO_2 adsorption properties. Installing the phosphane oxide functional group within the sterically restricted environment of the *m*-terphenyl backbone was expected to leave the P═O oxygen atom uncoordinated after the synthesis of the MOF. Fig. 2 gives an overview of the linker molecules and derived MOFs described herein.

Experimental

For synthetical details, analytical methods, and *in silico* methods, please refer to ESI.† Details on single crystal X-ray structure analyses on MOFs and linker molecule precursor compounds as well as full information on literature surveys regarding MOFs featuring the *m*-terphenyl structural motif are also given therein.

UHM-60

In a rubber-sealed screw vial, the linker molecule **4a** (66 mg, 0.14 mmol) and $Cu(NO_3)\cdot 2.5\ H_2O$ (132 mg, 568 μmol) were dissolved in *N*,*N*-dimethylacetamide (DMA; 14 mL). An aqueous solution of HBF_4 (48 wt%, 0.17 mL, 1.3 mmol) was added and the solution was placed in an oven at 75 °C for 5 d. The solution was filtered using a syringe filter, placed in a Schott bottle, and further reacted at 75 °C. After additional 2 d, a light blue powder had separated from the reaction solution. The liquid was removed *via* syringe, the solid added with fresh DMA (10 mL) and the mixture left standing for three hours before the liquid was again removed *via* syringe. After drying at 60 °C for 18 h, 110 mg of the as-synthesised sample were obtained.

UHM-61

In a rubber-sealed screw vial, the linker molecule **4b** (192 mg, 386 μmol) was dissolved in *N*,*N*-dimethylformamide (DMF; 10.6 mL). A solution of $Cu(NO_3)_2\cdot 3\ H_2O$ (100 mg mL^{-1} in demineralised water; 3.88 mL, 388 mg, 1.61 mmol, 4 eq.) and nitric acid (w = 20%; 0.86 mL, 3.0 mmol, 8 eq.) were added. The mixture was heated at 50 °C for 4 d. The mixture was cooled to room temperature, and the light blue solid isolated *via* filtration. The solid was washed with DMF (5 mL) and dried at 60 °C for 18 h.

UHM-62

In a crimp vial, the linker molecule **4c** (10 mg, 20 μmol) and $Cu(NO_3)_2\cdot 2.5\ H_2O$ (10 mg, 43 μmol, 2.2 eq.) were dissolved in a mixture of DMA (1.1 mL) and water (0.5 mL). 0.02 mL of hydrochloric acid (w = 32%) were added. The vial was sealed, and the mixture reacted at 85 °C for 4 d. Dark blue crystals suitable for X-ray structure determination were obtained. After a single crystal had been picked, the remaining crystals were isolated *via* filtration, repeatedly washed with small volumes of DMA (totalling 5 mL), and dried at 60 °C for 2 d. 15 mg of blue crystals were obtained. For characterisation purposes, the syn-

thesis was scaled up to 200 mg of linker molecule. In a typical reaction, 200 mg of linker molecule (392 μmol), 191 mg of $Cu(NO_3)_2{\cdot}2.5\ H_2O$ (821 μmol, 2.1 eq.), 13 mL DMA, 8 mL H_2O, and 0.40 mL hydrochloric acid (w = 32%) were used. After 3 d, 203 mg of a polycrystalline light blue solid were obtained and washed/dried as described above.

UHM-63

In modification of the procedure described for **UHM-62**, the linker molecule **4d** (10 mg, 16 μmol) and $Cu(NO_3)_2{\cdot}2.5\ H_2O$ (10 mg, 43 μmol, 2.7 eq.) were reacted in a 1 : 1 mixture of DMA and water (total volume of 0.80 mL). 13 mg of single crystals suitable for X-ray structure determination were obtained after 3 d. The synthesis was scaled up to use 201 mg of linker molecule (398 μmol), 166 mg of $Cu(NO_3)_2{\cdot}2.5\ H_2O$ (714 μmol), 13 mL DMA, 8 mL H_2O, and 0.40 mL hydrochloric acid (w = 32%). After 4 d, 239 mg of a polycrystalline light blue solid were obtained.

Results and discussion

Characterisation of UHM-60

The structure of **UHM-60** with a composition of Cu_2L reflecting a neutral framework was elucidated using homology modelling on the **UHM-25**[27] structure (see ESI† for details). When disregarding the phosphorus functional group, **UHM-60** can be described in the cubic space group $Pm\bar{3}m$ with a = 25.93 Å. The activation procedure of sequential solvent exchange and final thermal activation *in vacuo* gave a permanently porous material as proven by nitrogen physisorption at 77 K and the retention of characteristic reflections in powder X-ray diffraction (pXRD) at the desolvated state. A type I(b) isotherm indicative of a microporous adsorbent featuring wider micropores was obtained, and a specific BET surface area of S_{BET} = 1939 $m^2\ g^{-1}$ as well as a total pore volume of 0.89 $cm^3\ g^{-1}$ were derived. Based on a structural model obtained from homology modelling, a calculation using the Poreblazer software[28] suggests a void volume of 76% and an accessible specific surface area of 1950 $m^2\ g^{-1}$. TG-DTA/MS measurements of as-synthesised and activated materials have proven the near-quantitative removal of solvent guest molecules and a thermal stability of **UHM-60** up to approximately 220 °C.

The residue of thermal analysis was characterised as $Cu_4O(PO_4)_2$ from X-ray powder diffraction. The linker integrity was proven by NMR spectroscopy on the reisolated linker molecule from acidic MOF digestion.

Characterisation of UHM-61

UHM-61 is isostructural to **UHM-60** as shown by pXRD (a = 25.96 Å). The cubic symmetry is reflected by the morphology of the material as revealed from scanning electron microscopy showing the presence of cubes with an edge length of approximately 25 μm. The linker identity was examined *via* ^1H and $^{31}P\{^1H\}$ NMR spectroscopy on an acid-digested sample of **UHM-61**. We found a mixture of phosphane sulfide linker molecule and phosphane oxide linker molecule in a ratio of approximately 2 : 1, proving that some oxidation of the P═S functional group took place, presumably during the synthesis of the MOF. Physisorption experiments employing N_2 at 77 K and Ar at 87 K gave type I(b) isotherms and let us derive specific surface areas of S_{BET} = 1930 $m^2\ g^{-1}$ and 1772 $m^2\ g^{-1}$, respectively. The total pore volume was determined to be 0.78 $cm^3\ g^{-1}$ from N_2 physisorption. A Poreblazer calculation suggests a void volume of 76% and an accessible specific surface are of 1879 $m^2\ g^{-1}$ for **UHM-61**. TG-DTA/MS in an oxidising atmosphere verified the release of SO_2 during the combustion of the material starting from 220 °C, demonstrating the incorporation of the sulfur-containing functional group into the material. To the best of our knowledge, **UHM-61** is the first MOF employing a linker molecule featuring the phosphane sulfide functional group.

Structural description of UHM-60/UHM-61

Fig. 3 shows the relevant structural representations of **UHM-60** and **UHM-61**. The structure shown in Fig. 3a is best understood when pore-discriminating polyhedra with respective vertices provided by Cu(II) paddle-wheels are identified. Cuboctahedra (Fig. 3b; orange colour) with an edge length of 9.2 Å are interconnected along the spatial dimensions *via* four linker molecules, respectively (Fig. 3c; green colour). Those bridges form a square cuboid of dimensions 9.2 Å × 9.2 Å × 12.9 Å. The $PEMe_2$ (E = O, S) functional groups exclusively extending into this pore type show a very dense packing, presumably exhibiting non-classical hydrogen bonding features of type P═E···H–CH_2–P. Another pore type described by a rhombicuboctahedron (Fig. 3d; red colour) is framed by orange- and green-type pores to construct a cube with cuboctahedra placed at the eight vertices and the bridges as edges of the cube. The faces of the cube represent pore windows (large blue sphere, Fig. 3a) connecting neighbouring red-type pores.

Within **UHM-60**/**UHM-61** as well as an isoreticular Cu(II)-based MOF by Zaworotko and co-workers[29] and the **UHM-25** class materials reported by our group,[27] the tip of the 'V' of the V-shaped linker extends into the red-type pores, thus being averted from the volume of green-type pores. In contrast to **UHM-60**/**UHM-61**, where the P-based functional groups extend into the green-type pores, the **UHM-25**-class MOFs show substitution with chiral pool-derived functional groups expanding into the readily accessible red-type pores.

Topology

The underlying net of **UHM-60** and **UHM-61** can be described as binodal (3,4)-c **ucp** with minimal transitivity[30] *pqrs* = 2244. If the linker molecule is recognised as a single 4-c node, the edge-transitive and uninodal 4-c basic net **rhr** with *pqrs* = 1132 is obtained. The molecular (non-periodic) relative to the cuboctahedron shown in Fig. 3b, MOP-1, which is constructed from isophthalate ligands coordinated to Cu(II) paddle-wheels, was already presented in 2002.[31] O'Keeffe and Yaghi proposed different ways to interconnect cuboctahedra, depending on whether neighbouring cuboctahedra point at each other in a

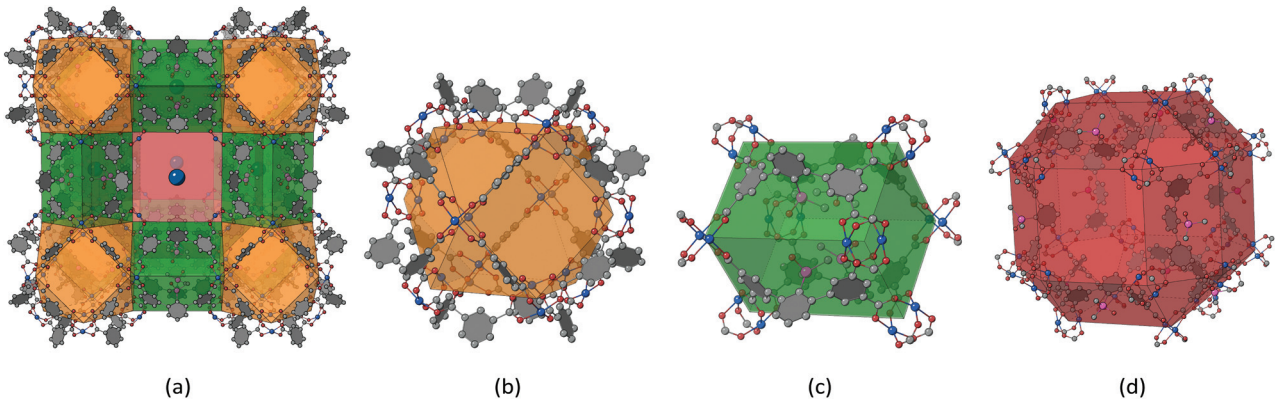

Fig. 3 Structural representations of **UHM-60** (**UHM-61** is isostructural). (a) View onto the *ab* plane with pore-discriminating polyhedra using Cu(II) paddle-wheels as vertices. Large blue spheres indicate pore windows between two neighbouring red-type pores. (b) The orange-type pores can be described by a cuboctahedron. (c) Green-type pores are best described by a square cuboid. (d) Red-type pores are represented by a rhombicuboctahedron. Guest molecules, axially coordinated ligands of Cu(II) paddle-wheels, and H atoms omitted for clarity. Fractional coordinates of centroids of polyhedra and the large blue sphere in space group $Pm\bar{3}m$: orange (0.5,0.5,0.5), green (0.5,0.5,0), red (0,0,0), blue (0.5,0,0). Aryls are shown as face-filled disks. Grey: C, red: O, purple: P, blue: Cu.

face-to-face (A), vertex-to-vertex (B), or vertex-to-face fashion (C).[32] Mixed combinations are realised in **zmj** (A and B) and **zhc** (A and C) topologies, respectively, while the exclusive presence of the simplest connection of type (A) is described in **ucp** topology. We discussed the implications of linker conformation on the resulting type of interconnectivity of neighbouring cuboctahedra earlier[27] and will expand this approach later herein.

UHM-62 and UHM-63

Characterisation of UHM-62 and UHM-63. The isostructural MOFs **UHM-62** and **UHM-63** crystallise in the orthorhombic space group *Immm*. Reisolation and NMR spectroscopic characterisation of the respective linker molecules after acidic digestion of the MOFs gave no indication of decomposition. TG-DTA/MS measurements show that the materials are stable up to approximately 250 °C and prove the successful removal of guest molecules. N_2 physisorption at 77 K gave type I(b) isotherms in both cases, with BET surface areas of 1429 $m^2\ g^{-1}$ and 1358 $m^2\ g^{-1}$ and total pore volumes of 0.68 $cm^3\ g^{-1}$ and 0.62 $cm^3\ g^{-1}$ for **UHM-62** and **UHM-63**, respectively. The Ar physisorption isotherm at 87 K for **UHM-62** also shows type I(b) behaviour and gave a specific surface area of S_{BET} = 1457 $m^2\ g^{-1}$. A void volume of 73% (74%) and a specific surface area of 1337 $m^2\ g^{-1}$ (1199 $m^2\ g^{-1}$) was calculated using Poreblazer for **UHM-62** (**UHM-63**). For both materials, characteristic reflections are retained at the desolvated state as shown by pXRD, underlining the retention of structural integrity. When disregarding axially coordinated Cu(II) ligands, both materials are electrostatically neutral compounds with a general composition of Cu_2L.

Structural description of UHM-62/UHM-63. The structure shall be described in terms of the different pore types identified and visualised in Fig. 4c–f. With respect to the centroids of limiting Cu(II) paddle-wheels, the principal geometry of pores depicted in Fig. 4c–e can be described by rectangular cuboids of dimensions 16.7 Å × 12.9 Å × 9.2 Å. The longer two of the respective edges represent the interconnection of paddle-wheels across the linker molecule, while the distance of 9.2 Å corresponds to a linkage by an isophthalate entity. The orange-type pore (Fig. 4c) shows additional symmetrical attachment of two edges to opposing faces of 16.7 Å × 12.9 Å with an edge-to-edge distance of 18.3 Å. Pore types depicted in green (Fig. 4d) and yellow colour (Fig. 4e) contain no phosphorus-based functional groups. The yellow-type pore shows additional capping by two vertices attached to opposing faces of 12.9 Å × 9.2 Å with a vertex-to-vertex distance of 26.0 Å. The pore type indicated by a large blue sphere (Fig. 4f) is framed by four linker molecules with phosphane oxide oxygen atoms at distances of 3.7 Å and 7.8 Å, respectively. Remarkably short Cu···Cu inter-paddle-wheel distances of 4.8227(13) Å (**UHM-62**) and 4.789(3) Å (**UHM-63**), respectively, have been found within the materials. In **UHM-62**, the interstitial space was found to be occupied by a μ^2-Cl^- ion. Within **UHM-63**, a mixed occupation by Cl^- and an oxygen-type ligand, presumably water, with an occupancy of 0.53(3) for Cl^- was found. In both cases, charge-neutralising dimethylammonium cations were located from the difference Fourier map. To date, no attempts were made to exchange the O/Cl^--type interstitial sites against each other or for related chemical species or to assess the potential removal of the bridging ligands. The highly polar environment characterised by electropositive Cu(II) ions and the negatively polarised phosphane oxide oxygen atoms might render this unique chemical environment interesting in applications such as gas storage or separation or studies concerning the magnetic interaction between inter-paddle-wheel Cu(II) ions.

Shortest inter-paddle-wheel distances for MOFs based on the *m*-terphenyl tetracarboxylate linker molecule have been found for Zn(II)-based (Zn···Zn = 3.751(4) Å) and Mn(II)-based (Mn···Mn = 3.892(2) Å) materials.[33] Herein, a 2′-aza-functionalized *m*-terphenyl diisophthalate linker molecule was used and the paddle-wheels were bridged by μ^2-H_2O ligands. In

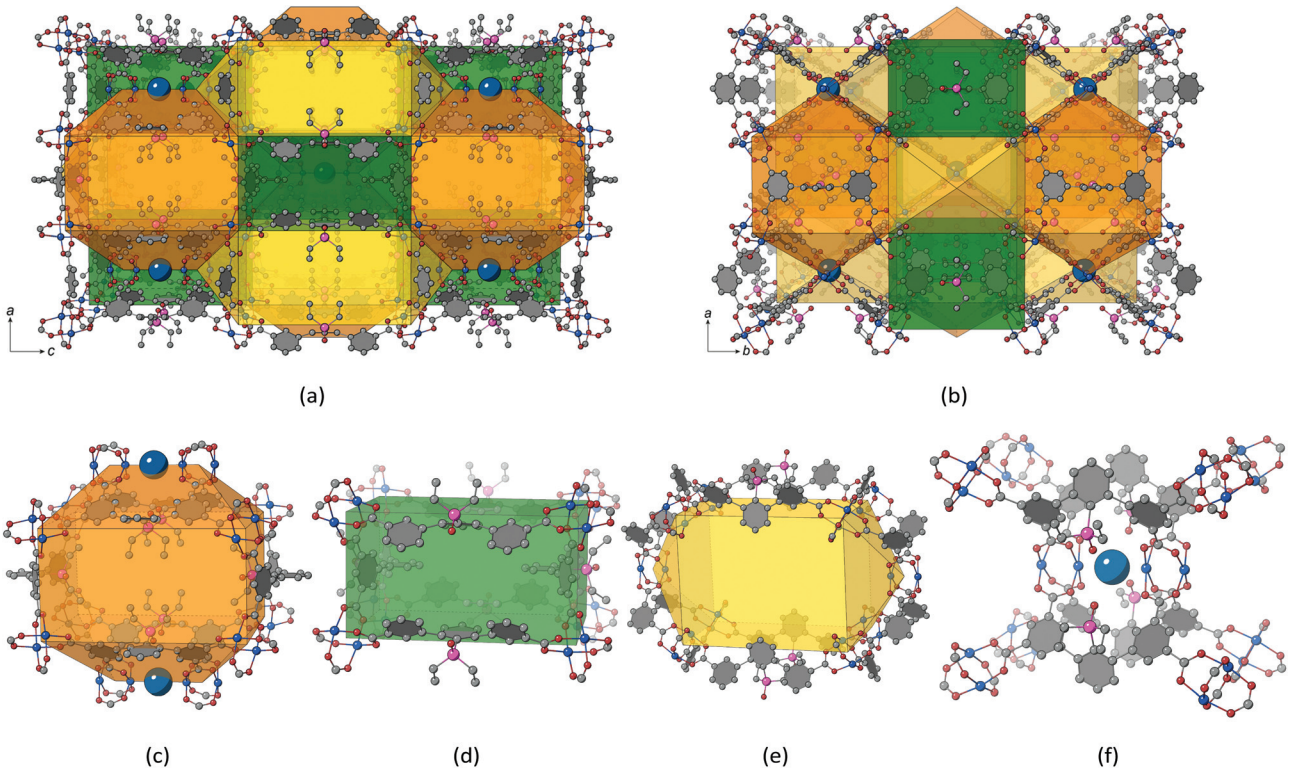

Fig. 4 Structure of **UHM-62** (**UHM-63** is isostructural) with pore-discriminating coordination polyhedra and large blue spheres with adjacent Cu(II) paddle-wheels as vertices (a) looking onto the *ac* plane and (b) onto the *ab* plane. (c) Orange-type pores are described by a rectangular cuboid with two edges added to opposing faces, (d) green-type pores by a rectangular cuboid. (e) Pores indicated by yellow colour can be described by an elongated square bipyramid. (f) A blue sphere indicates interstitial space between two neighbouring Cu(II) paddle-wheels which are interconnected by four linker molecules. An idealised activated state of the material omitting H atoms, guest molecules, and Cu-coordinated moieties is shown. Fractional coordinates of the polyhedral centroids and the blue sphere within the space group *Immm*: blue (0,0,0), green (0.5,0,0.5), yellow (0,0,0.5), orange (0,0.5,0.5). *m*-Terphenyl backbone aryls shown as grey disks. Grey: C, red: O, purple: P, blue: Cu.

Zhou and co-workers' **PCN-88**, which is isoreticular to **UHM-62**/**UHM-63** (see section below) employing the elongated 2,7-bis(3′,5′-dicarboxyphenyl)naphthalene linker molecule, an inter-paddle-wheel Cu···Cu distance of 7.3655(12) Å was found.[34] This cavity proved to be efficient as a single-molecule trap (SMT) for CO_2, rendering the material promising in terms of CO_2 capture or activation. Recently, the **PCN-88** topology was first found within a Cu(II) *m*-terphenyl tetracarboxylate-based material **BUT-301** [35] by employing the 5′-NO_2-substituted linker molecule with Cu···Cu = 4.7575(13) Å and a μ^2-chloride ion. In addition, we are aware of only few examples with axially cross-linked Cu(II) paddle-wheels of 3-periodic MOFs where the link is provided by a chloride anion[36] (Cu···Cu = 4.550(3) Å) or an oxygen-type ligand. Liu *et al.* found a water molecule cross-linking neighbouring Cu(II) paddle-wheels at a distance of 4.481(2) Å.[37]

Carbon dioxide and methane physisorption and selectivities

The chemical nature of the P═O bond is not sufficiently described in terms of a simple Lewis structure, as Gilheany pointed out in an influential review.[38] In order to assess the influence of the accessible and polar phosphoryl functional group, we evaluated **UHM-62** as a model compound for the study of adsorption and separation of carbon dioxide and methane, with the former having a large quadrupolar moment. The CO_2 and CH_4 adsorptions at 273 K and 298 K for **UHM-62** are shown in Fig. 5a.

CO_2 uptakes of 84.0 cm^3 (STP) g^{-1}/3.72 mmol g^{-1} (298 K) and 114.2 cm^3 (STP) g^{-1}/5.06 mmol g^{-1} (273 K) were determined, whereas 16.4 cm^3 g^{-1}/0.722 mmol g^{-1} and 24.0 cm^3 g^{-1}/1.06 mmol g^{-1} of CH_4 are adsorbed at 298 K and 273 K, respectively. Isosteric heats of adsorption (Q_{st}) at low coverage were determined to be 28.9 kJ mol^{-1} and 16.0 kJ mol^{-1} for CO_2 and CH_4, respectively (Fig. 5b).

A comparison with literature-known Cu(II)-based MOFs based on the *m*-terphenyl linker molecule reveals that CO_2 capacities up to 122.6 cm^3 g^{-1} at 298 K (ref. 39) and Q_{st} values up to 39.5 kJ mol^{-1} (ref. 40) with median values of 103 cm^3 g^{-1} and 24.6 kJ mol^{-1}, respectively, were found. While the Q_{st} value found for **UHM-62** lies in the upper quintile, the total CO_2 uptake is the second lowest of the values reported in literature. The highest adsorption enthalpies have been reported for materials with 5′-F-2′-NH_2 (39.5 kJ mol^{-1}),[40] 2′-NH_2 (37.51 kJ mol^{-1}),[11] and 2′-aza-functionalized *m*-terphenyls (36.9 kJ mol^{-1}),[9] indicating a strong interaction between the nitrogen-based functional groups and CO_2. A notable excep-

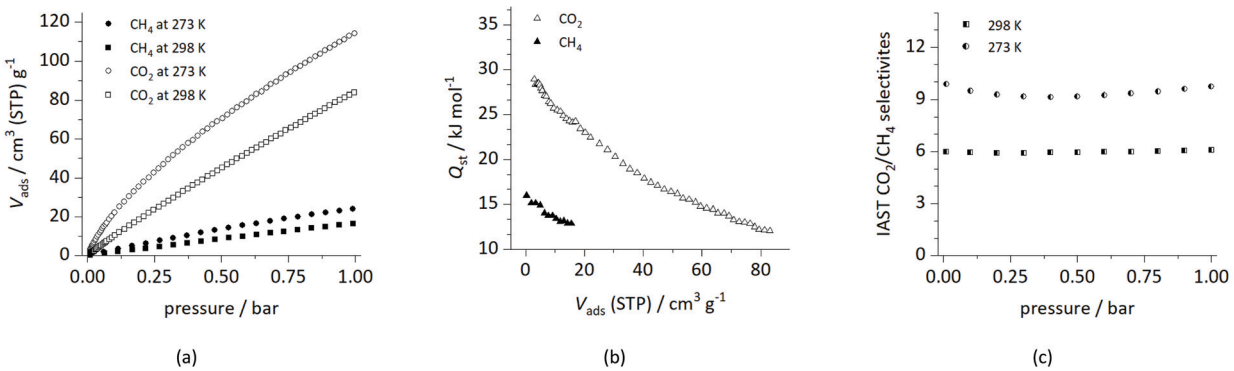

Fig. 5 (a) Adsorption branches of CO_2 and CH_4 physisorption experiments on **UHM-62** at temperatures of 273 K and 298 K, respectively. (b) Isosteric heats of adsorption Q_{st} for CO_2 and CH_4, respectively. (c) IAST selectivity plot for a binary CO_2/CH_4 = 50/50 mixture at 273 K and 298 K, respectively.

tion is found with **ZJNU-54** with a 2′-NH_2-4′,6′-diaza substitutional pattern, where a moderate value of 24.7 kJ mol^{-1} was found. However, substitution with nitrogen-based functional groups at positions other than 2′ generally gave rather medium Q_{st} values between 20.7 kJ mol^{-1} and 26.72 kJ mol^{-1}.[4,39,41–44] For electrostatically neutral MOFs featuring unsubstituted and alkyl-substituted *m*-terphenyl linker molecules, Q_{st} values between 22.5 kJ mol^{-1} and 24.8 kJ mol^{-1} were found.[4,6,14] For **PCN-88**, Q_{st} = 27 kJ mol^{-1} and a capacity of 94 cm^3 g^{-1} (296 K) were reported.[34] Taken all together, there is indication for an increased interaction between the P═O functional group and CO_2 as indicated by an increased Q_{st} value compared to unfunctionalized materials, but the total CO_2 uptake was found to be comparably low. This might be attributed to reduced surface area and pore volume, which are necessary prerequisites for significant CO_2 capacities.

The ideal adsorbed solution theory (IAST)[45] was used to calculate the CO_2/CH_4 selectivities of **UHM-62** at 298 K and 273 K, respectively (Fig. 5c). Selectivities of 6.1 (298 K) and 9.7 (273 K) at 1 bar were obtained. Within the group of Cu(II)-based *m*-terphenyl MOFs, best selectivities were determined for anionic **JLU-Liu22**[46] (9.4 at 298 K) and a cationic MOF[9] (30.8 at 298 K). Within the subset of neutral MOFs, selectivities between 4.95 and 7.14 at 298 K were reported; **UHM-62** is thus expected to show only modest selectivities in CO_2/CH_4 separation processes according to the IAST model. For a detailed tabulation of literature-available data regarding CO_2/CH_4 capacities and selectivities, see Tables S6 and S7.†

Topology of UHM-62 and UHM-63. **UHM-62** and **UHM-63** can be deconstructed in several ways shown in Fig. 6a–c in terms of their augmented nets. The Cl^- ion (**UHM-62**) as well as the site of mixed occupancy of Cl^- and an oxygen atom species (**UHM-63**) can (a) be omitted during the deconstruction procedure, (b) be regarded as a link between two 4-c nodes, rendering those to become a set of two interconnected 5-c nodes, or (c) be taken as a chemical conjunction between the paddle-wheels, thus contracting two 4-c nodes to a single 8-c node. The corresponding nets in terms of TOPOS symbols or, if available, RCSR symbols (three-letter codes set in bold lettering), can be identified as:

(a) 3,3,4,4T199: a (3,3,4,4)-c net with *pqrs* = 4564
(b) **tim**: a (3,3,4,5)-c net with *pqrs* = 4653
(c) **tst**: a (3,3,4,8)-c net with *pqrs* = 4553

It is noteworthy to mention that the nets of 3,3,4,4T199 and the commonly encountered **mfj** are closely related to each other as can be seen from the comparison made in Fig. 6d and e. Both nets are (3,3,4,4)-c and derived from two different (4,4,4,4)-c nets, however, the spatial arrangement of the 4-c nodes depicted in dark blue colour in Fig. 6d–e differs significantly. A stacked orientation is observed for the former, while for **mfj** a parallel-displaced alignment is found.

Conformations of *m*-terphenyl diisophthalates and topology of derived Cu(II)-based MOFs

An evaluation of literature-known three-periodic MOFs employing the *m*-terphenyl diisophthalate linker molecule and its substituted derivatives (Table S4†) has shown that there is, apart from only relatively few exceptions that came to our attention,[8,9,35,47–49] a strong preference to form structures with underlying **mfj** or **sty** topologies, with the first examples reported in literature being the **PCN-305** to **PCN-308** series[4] for **mfj** and a material that has been prepared by post-synthetic metal ion exchange of Zn(II) for Cu(II) for **sty**.[11] The replacement of the phosphorus-attached methyl groups (**UHM-60**/**UHM-61**) for ethyl (**UHM-62**) and phenyl groups (**UHM-63**) was expected to inevitably implicate a change in topology. It was our intention to increase the steric demands of the 2′ substituent to render the close packing of the P-attached functional groups within the bridges described in **ucp** topology (see Fig. 3c) less likely. Nevertheless, the fact that a new topology (**ucp**) and one that has only been realised once so far (3,3,4,4T199) for MOFs belonging to the well-established class of Cu(II) *m*-terphenyl diisophthalate MOFs, let us assume that there is an additional structure–topology relationship to be considered.

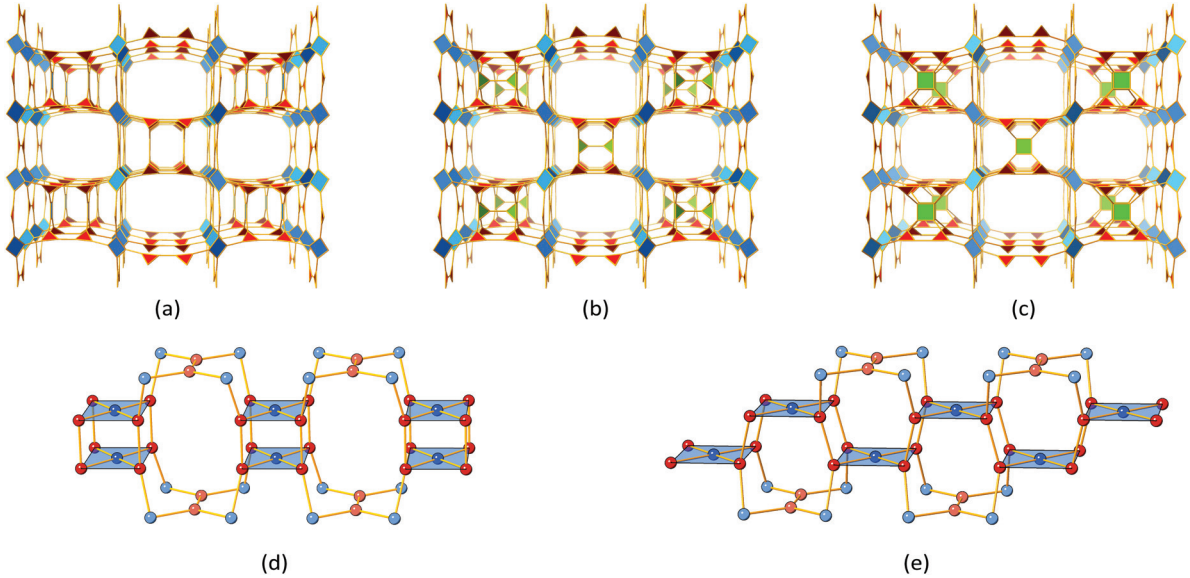

Fig. 6 (a–c) show possible representations of underlying augmented nets of **UHM-62** and **UHM-63** according to the possibilities proposed in the text where 3-c nodes are shown in red and 4-c nodes are shown in blue colour. Symmetry-inequivalent 3-c and 4-c nodes are not further distinguished by colour. (a) Augmented version of 3,3,4,4T199. (b) **tim-a** features sets of interconnected 5-c nodes depicted as green-coloured square pyramids in a (3,3,4,5)-c underlying net. (c) In **tst-a**, 8-c nodes represented by green cubes of a (3,3,4,8)-c net are present. (d) and (e) compare the nets (d) 3,3,4,4T199 and (e) **mfj** where topologically inequivalent 3-c and 4-c notes are distinguished by different shades of red and blue colour, respectively. Dark blue 4-c nodes have been added with a translucent square with neighbouring 3-c nodes as edges. It becomes obvious that 3,3,4,4T199 shows a stacked fashion of the 4-c nodes in question, while for **mfj** a stepped sequence is observed.

We tried to assess and classify the conformations of *m*-terphenyl diisophthalate linker molecules in order to derive implications on resulting topologies. Therefore, we determined the fold and twist angles between the least-squares mean planes (LSMPs) of isophthalates belonging to the same linker molecule. In comparison to an ordinary interplanar angle (plane-to-plane angle), its deconstruction into components of twist and fold is useful for an interpretation in terms of chemical meaningfulness. The twist angle is a measure for the torsion of the isophthalates along the centroid–centroid connecting line, while the fold angle quantifies the opening angle of the isophthalates with respect to their connecting chemical entity, *e.g.* an aryl for *m*-terphenyl-type linker molecules. Fig. 7a and b show folded and twisted conformations of a *m*-terphenyl linker molecule, respectively. For a graphical description of twist and fold angles, see ESI.† LSMPs as well as the relevant angles can conveniently be examined using the OLEX2 software.[50]

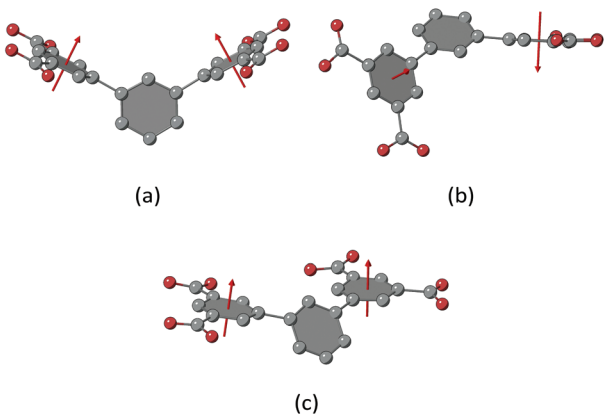

Fig. 7 (a) Folded, (b) twisted, and (c) coplanar conformations of the *m*-terphenyl diisophthalate linker molecule. Aryls are shown as grey disks, H atoms have been omitted for clarity. The plane normals of the diisophthalates are shown as red arrows.

The results of our survey are visualised in Fig. 8. It can be recognised that two linker conformations are present within **mfj** topology. One conformer shows twist angles between 72°–75° and a fold component of 28°–34° and is thus referred to as twisted conformer. A second, folded conformer shows twist angles of 0° and fold angles of 54°–66°. It is noteworthy that isophthalates related by mirror-symmetry cannot exhibit twist angles other than 0°. Within the MOFs with underlying **sty** topology, only the folded conformation of the linker molecule with twist angles being close to 0° and a fold component between 60°–71° is observed. For the UHM series materials **UHM-60** to **UHM-63**, twisting of the isophthalates is suppressed by the presence of sterically demanding tetrahedral organophosphorus functional groups attached to C2′. For **UHM-60**/**UHM-61** with underlying **ucp** topology, a folded conformation of the peripheral aryls with a fold angle of 51° is required. The fold angle for the linker conformation within **UHM-60**/**UHM-61** is slightly lower than that within folded conformations within for **mfj** (54°–66°) and **sty** (60°–71°) topologies.

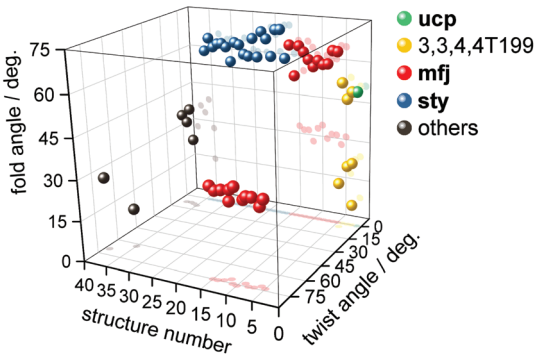

Fig. 8 Evaluation of fold and twist angles of isophthalates belonging to the same linker molecule within Cu(II) MOFs employing the *m*-terphenyl diisophthalate linker molecule and its substituted derivatives for literature-known examples as well as for **UHM-60**/**UHM-61** (structure number 1), **UHM-62** (2), and **UHM-63** (3). The different sphere colours represent **ucp** (green), 3,3,4,4T199 (yellow), **mfj** (red), **sty** (blue), or other (black) topologies. MOFs belonging to the structure numbers referred herein and corresponding angles are listed in Table S5.†

Also, for **UHM-62** and **UHM-63** with underlying 3,3,4,4T199 topologies, folded conformations of the linker molecule are observed. The first one shows fold components of 48.0(4)° and 50.8(3)° (for **UHM-62** and **UHM-63**, respectively), thus lying in a range close to that of **UHM-60**/**UHM-61**. The second conformer exhibits fold angles of 7.8(16)°/24.1(15)° (two disordered sites within **UHM-62**) and 22.7(5)° (**UHM-63**), which results in the isophthalates showing an approximately coplanar orientation. These values are also confirmed by the isoreticular **BUT-301**, where fold angles of 53.7(2)° for the folded conformer and 16.96(19)° for the coplanar conformer are found. To the best of our knowledge, the coplanar conformation of peripheral aryls is first realised within *m*-terphenyl diisophthalate MOFs based on the 3,3,4,4T199 topology. Fig. 7c shows the coplanar conformation of the *m*-terphenyl diisophthalate linker molecule as discussed before. It is noteworthy that the transition from a folded conformation towards a coplanar conformation implies an increase in the metal-to-metal distances across the linker. For **UHM-62**, a distance between paddle-wheel centroids of 12.9 Å was found for the folded conformation, while the distance is increased to 16.7 Å within the coplanar conformation. It is obvious that the conformation of the *m*-terphenyl diisophthalates thus exerts direct and significant influence on the pore dimensions expected in a synthesised MOF.

For the examples of MOFs showing underlying nets not belonging to the four topologies discussed before, combinations of twist and fold contributions lying outside the ranges defined for **mfj**, **sty**, **ucp**, and 3,3,4,4T199 are observed, except for one example with an underlying topology characterised by a point symbol $\{6^2{\cdot}8^2{\cdot}12^2\}\{6^2{\cdot}8\}_4\{6^4{\cdot}8^2\}$ showing only a twisted conformation of the linker molecule.[8] The relevant angles discussed before are summarised in Table 1.

Table 1 Topologies observed for Cu(II)-based *m*-terphenyl diisophthalate MOFs. Angular ranges have been rounded. For exact values and corresponding references, see Table S5†

Topology	Conformer	Twist angles/deg.	Fold angles/deg.
mfj	Twisted	72–75	28–34
	Folded	0	54–66
sty	Folded	0	57–71
ucp	Folded	0	51
3,3,4,4T199	Folded	0	48–54
	Coplanar	0–4	8–23
3,3,3,4,4T31		62	14
		10	27
$\{6{\cdot}8{\cdot}9\}_4\{6{\cdot}8^4{\cdot}11\}\{6{\cdot}8^4{\cdot}12\}$		9	39
3,3,4T213		8	33
3,3,4,4T234		8	36
$\{6^2{\cdot}8^2{\cdot}12^2\}\{6^2{\cdot}8\}_4\{6^4{\cdot}8^2\}$	Twisted	70	27

Conclusions

We successfully synthesised *m*-terphenyl diisophthalate linker molecules with C2′-organophosphorus substituents. The dimethylphosphoryl and dimethylphosphane sulfide linker molecules **4a** and **4b**, respectively, gave the isostructural Cu(II)-based **UHM-60** and **UHM-61** with the relatively rare underlying **ucp** topology where the latter represents the first example of a MOF incorporating phosphane sulfide functional groups. The non-accessible P═E (E = O, S) functional group was made available to the pore volume by replacement of the P-attached methyl groups by ethyl and phenyl groups to give the Cu(II)-based **UHM-62** und **UHM-63**, respectively. These materials are examples of the rare underlying 3,3,4,4T199 topology and, in comparison to the isoreticular **PCN-88**, show a significant reduction of inter-paddle-wheel distances to 4.8227(13) Å and 4.789(3) Å, respectively. The chemical interconnection of the paddle-wheels allowed us to derive the topological types **tim** and **tst**. A study of CO_2 and CH_4 adsorption on **UHM-62** revealed very low influence of the highly polar P═O functional group on CO_2/CH_4 selectivities according to the IAST model and adsorption enthalpies. However, a comprehensive study of Cu(II)-based MOFs employing the *m*-terphenyl diisophthalate linker molecule by deconstruction of interplanar angles to components of twist and fold allowed for the classification of linker conformations and might be useful in the systematic exploration of rare or previously unknown topologies by chemical restriction of conformational space.

Conflicts of interest

There are no conflicts to declare.

Notes and references

1 C. A. Tolman, *Chem. Rev.*, 1977, **77**, 313–348.
2 A. M. Wilson, P. J. Bailey, P. A. Tasker, J. R. Turkington, R. A. Grant and J. B. Love, *Chem. Soc. Rev.*, 2014, **43**, 123–134.

3 L. Ortega-Moreno, M. Fernández-Espada, J. J. Moreno, C. Navarro-Gilabert, J. Campos, S. Conejero, J. López-Serrano, C. Maya, R. Peloso and E. Carmona, *Polyhedron*, 2016, **116**, 170–181.
4 Y. Liu, J.-R. Li, W. M. Verdegaal, T.-F. Liu and H.-C. Zhou, *Chem. – Eur. J.*, 2013, **19**, 5637–5643.
5 Z. Lu, L. Du, K. Tang and J. Bai, *Cryst. Growth Des.*, 2013, **13**, 2252–2255.
6 D.-L. Chen, Z. Tian, Y. He, M. He, L. Zhu, H. Zhong, X. Zhang, Y. Wang and Y. Zhang, *Dalton Trans.*, 2018, **47**, 2444–2452.
7 L. Fan, W. Fan, B. Li, X. Liu, X. Zhao and X. Zhang, *CrystEngComm*, 2015, **17**, 4669–4679.
8 J. Liu, W. Wang, Z. Luo, B. Li and D. Yuan, *Inorg. Chem.*, 2017, **56**, 10215–10219.
9 B. Liu, H.-F. Zhou, L. Hou, Z. Zhu and Y.-Y. Wang, *Inorg. Chem. Front.*, 2016, **3**, 1326–1331.
10 J. Jiao, L. Dou, H. Liu, F. Chen, D. Bai, Y. Feng, S. Xiong, D.-L. Chen and Y. He, *Dalton Trans.*, 2016, **45**, 13373–13382.
11 T. K. Pal, D. De, S. Neogi, P. Pachfule, S. Senthilkumar, Q. Xu and P. K. Bharadwaj, *Chem. – Eur. J.*, 2015, **21**, 19064–19070.
12 M. Gupta, D. De, K. Tomar and P. K. Bharadwaj, *Inorg. Chim. Acta*, 2018, **482**, 925–934.
13 A. K. Gupta, D. De, K. Tomar and P. K. Bharadwaj, *Dalton Trans.*, 2018, **47**, 1624–1634.
14 Y. He, X. Gao, Y. Wang, M. He and S. Li, *Dalton Trans.*, 2018, **47**, 8983–8991.
15 J. E. Reynolds III, S. G. Dunning, C. M. McCulley and S. M. Humphrey, in *Elaboration and Applications of Metal-Organic Frameworks*, ed. S. Ma and J. A. Perman, World Scientific Publishing Co. Pte. Ltd., Singapore, Shengqian, 2018, pp. 37–142.
16 Q.-D. Shu, S.-N. Kong, Y.-Z. Wei and M.-H. Shu, *Polyhedron*, 2016, **118**, 96–102.
17 J. Feng, H. Li, Q. Yang, S.-C. Wei, J. Zhang and C.-Y. Su, *Inorg. Chem. Front.*, 2015, **2**, 388–394.
18 Y.-Y. Yang, Z.-J. Lin, J. Liang, Y. Huang and R. Cao, *CrystEngComm*, 2015, **17**, 4547–4553.
19 Y. Sun, X. Chen, F. Wang, R. Ma, X. Guo, S. Sun, H. Guo and E. V. Alexandrov, *Dalton Trans.*, 2019, **48**, 5450–5458.
20 H. Guo, Y. Sun, F. Zhang, R. Ma, F. Wang, S. Sun, X. Guo, S. Liu and T. Zhou, *Inorg. Chem. Commun.*, 2019, **107**, 107492.
21 A. M. Bohnsack, I. A. Ibarra, P. W. Hatfield, W. J. Yoon, Y. K. Hwang, J.-S. Chang and S. M. Humphrey, *Chem. Commun.*, 2011, **47**, 4899–4901.
22 X. Du, R. Fan, L. Qiang, K. Xing, H. Ye, X. Ran, Y. Song, P. Wang and Y. Yang, *ACS Appl. Mater. Interfaces*, 2017, **9**, 28939–28948.
23 Y. Li, Z. Weng, Y. Wang, L. Chen, D. Sheng, Y. Liu, J. Diwu, Z. Chai, T. E. Albrecht-Schmitt and S. Wang, *Dalton Trans.*, 2015, **44**, 20867–20873.
24 W. R. Lee, D. W. Ryu, W. J. Phang, J. H. Park and C. S. Hong, *Chem. Commun.*, 2012, **48**, 10847–10849.
25 L. Huo, J. Zhang, L. Gao, X. Wang, L. Fan, K. Fang and T. Hu, *J. Solid State Chem.*, 2017, **256**, 168–175.
26 R. Poloni, K. Lee, R. F. Berger, B. Smit and J. B. Neaton, *J. Phys. Chem. Lett.*, 2014, **5**, 861–865.
27 M. Sartor, T. Stein, F. Hoffmann and M. Fröba, *Chem. Mater.*, 2016, **28**, 519–528.
28 L. Sarkisov and A. Harrison, *Mol. Simul.*, 2011, **37**, 1248–1257.
29 C. Li, W. Qiu, W. Shi, H. Song, G. Bai, H. He, J. Li and M. J. Zaworotko, *CrystEngComm*, 2012, **14**, 1929.
30 M. Li, D. Li, M. O'Keeffe and O. M. Yaghi, *Chem. Rev.*, 2014, **114**, 1343–1370.
31 M. Eddaoudi, J. Kim, J. B. Wachter, H. K. Chae, M. O'Keeffe and O. M. Yaghi, *J. Am. Chem. Soc.*, 2001, **123**, 4368–4369.
32 M. O'Keeffe and O. M. Yaghi, *Chem. Rev.*, 2012, **112**, 675–702.
33 B. Liu, W.-P. Wu, L. Hou, Z.-S. Li and Y.-Y. Wang, *Inorg. Chem.*, 2015, **54**, 8937–8942.
34 J.-R. Li, J. Yu, W. Lu, L.-B. Sun, J. Sculley, P. B. Balbuena and H.-C. Zhou, *Nat. Commun.*, 2013, **4**, 1538.
35 M.-M. Xu, X.-J. Kong, T. He, X.-Q. Wu, L.-H. Xie and J.-R. Li, *Dalton Trans.*, 2019, **48**, 9225–9233.
36 F. Gao, Y. Li, Y. Ye, L. Zhao, L. Chen and H. Lv, *Inorg. Chem. Commun.*, 2017, **80**, 72–74.
37 J. Liu, G. Liu, C. Gu, W. Liu, J. Xu, B. Li and W. Wang, *J. Mater. Chem. A*, 2016, **4**, 11630–11634.
38 D. G. Gilheany, *Chem. Rev.*, 1994, **94**, 1339–1374.
39 D. Bai, X. Gao, M. He, Y. Wang and Y. He, *Inorg. Chem. Front.*, 2018, **5**, 1423–1431.
40 T. K. Pal, D. De, S. Senthilkumar, S. Neogi and P. K. Bharadwaj, *Inorg. Chem.*, 2016, **55**, 7835–7842.
41 Z. Lu, Y. Xing, L. Du, H. He, J. Zhang and C. Hang, *RSC Adv.*, 2017, **7**, 47219–47224.
42 Z. Lu, F. Meng, L. Du, W. Jiang, H. Cao, J. Duan, H. Huang and H. He, *Inorg. Chem.*, 2018, **57**, 14018–14022.
43 J. Jiao, D. Jiang, F. Chen, D. Bai and Y. He, *Dalton Trans.*, 2017, **46**, 7813–7820.
44 L. Zhang, K. Jiang, Y. Li, D. Zhao, Y. Yang, Y. Cui, B. Chen and G. Qian, *Cryst. Growth Des.*, 2017, **17**, 2319–2322.
45 A. L. Myers and J. M. Prausnitz, *AIChE J.*, 1965, **11**, 121–127.
46 D. Wang, B. Liu, S. Yao, T. Wang, G. Li, Q. Huo and Y. Liu, *Chem. Commun.*, 2015, **4**, 1166–1169.
47 D. Wang, B. Liu, S. Yao, T. Wang, G. Li, Q. Huo and Y. Liu, *Chem. Commun.*, 2015, **51**, 15287–15289.
48 Y. Pan, W. Liu, D. Liu, Q. Ding, J. Liu, H. Xu, M. Trivedi and A. Kumar, *Inorg. Chem. Commun.*, 2019, **100**, 92–96.
49 J. Jiao, H. Liu, F. Chen, D. Bai, S. Xiong and Y. He, *Inorg. Chem. Front.*, 2016, 1411–1418.
50 O. V. Dolomanov, L. J. Bourhis, R. J. Gildea, J. A. K. Howard and H. Puschmann, *J. Appl. Crystallogr.*, 2009, **42**, 339–341.